

VOID FRACTION IN HIGHLY TURBULENT AND LARGE DIAMETER HORIZONTAL PIPE FLOW

A. A. Lakis & Nguyen D. Trinh

*Department of Mechanical Engineering, École Polytechnique de Montréal.
C.P. 6079, Succ. Centre-Ville, Montréal, Québec, Canada H3C 3A7

ABSTRACT

This study presents an experimental correlation of void fraction distribution in large diameter horizontal pipe flow. A turbulent air-water mixture flows through a series of 8-in. diameter pipes, with a Reynolds number of 2.10^6 on a liquid basis and a 30% maximum flow volumetric quality under normal operating conditions. A double conical hot film probe has been designed to measure simultaneously the void fraction and the bubble velocity. The hot film probe has been calibrated in a 2-in. diameter pipe with bubble flow. Measured local void fractions have been corrected by the quick closing valves global method through an improved calibration procedure. Tests have been carried out along the pipe axis and in both cross-sectional planes. Fully-developed flow is identified at a distance more than 100 times pipe diameter from the mixer. Non-uniformity of the profiles is reviewed only in the transversal/transversal plane. Void measurements in the large-diameter horizontal pipe are found to be qualitatively comparable with numerical results in a 1.0-in. diameter horizontal pipe (Brown and Kranich [9, 43]). Two new sets of correlations are proposed here. The first predicts the longitudinal distribution of void fraction, where correlations are expressed in terms of axial location and flow volumetric quality. In the second, distribution of the void fraction in the transversal plane may be predicted either by a linear or an exponential model. Void fraction profiles are found to be almost flat in the radial/horizontal plane for which the power law may be assumed.

INTRODUCTION

The presence of the dispersed phase in a continuous flow is characterized by the proportion occupied by this phase along the flow. In an air-water mixture flow, this proportion represents the quasi-static fraction of air bubbles and is symbolized by α . Since the void fraction is a measure of the change in proportion resulting either from a variation in the dispersed phase or from interaction between phases, it represents an additional independent kinetic variable in the general expression of a two-phase flow. Information on the void fraction is indispensable in the evaluation of average mixture density, average kinetic energy of phases, pressure drop, momentum and mass transfer rates as well as in the detailed study of the mechanism of a mixture flow. Important industrial applications such as nuclear and bubble column reactors in nuclear and chemical industries, for example, currently need more data on the local flow profile.

Most practical applications deal with turbulent flow in which a variety of flow regimes exist. These make the measurement of the different flow parameters more complicated and limit the versatility of the instruments developed for the measurement of the various aspects of the two-phase flow.

The void fraction may be determined by several methods which have been proposed, notably the use of a resistive probe (Neal and Bankoff [1]), a hot wire anemometer (Hsu et al. [2]) or hot film (Delhaye [3]), the gamma ray method (Kazin [4], Teyssedou et al.[32], Thiagarajan et al.[33], Jiang et al. [34]), the optic taper method (Miller and Metchie [5]), lasers (Ohba et

al.[6]), optical fiber probe (Cartellier [35], Morris et al.[36], Serdula et al.[37]), impedance probe (Teyssedou et al. [38]), Yin-Pang et al. [39] and differential pressure (D/P) (Yin-Pang et al. [39]-[44]), capacitance method (Elkow [40]) or conductance method (Gupta et al. [41]) for the most part in air-water vertical flows.

In their results, Brown et al. [7] represented the void fraction profile of horizontal and vertical, bubble and slug, upward and downward flow in a 2.5-in. diameter tube, by equations of the parabolic type having a maximum value at the pipe wall. Zivi [8] expressed the rate of dissipation of energy of an annular flow in terms of the void fraction which is obtained after minimizing the dissipation of energy. Brown and Kranich [9] have obtained the void fraction and velocity profiles by simulating the modified conservation equations of a horizontal /vertical bubble flow in a 1.0-in diameter pipe with measurements of the pressure and the overall liquid fraction.

Using the finite-difference resistance modelling for liquid level measurement in stratified gas-liquid systems, Gupta et al. [41] propose a mathematical model for measurement of the void fraction. Measurements in 3-D with a conical hot film probe have also been presented by Wang et al. [10] in a small diameter pipe with vertical bubble flow. Chien et al. [42] study the effect of side-tube configuration on the void fraction measurement and their results show a good agreement for a void fraction < 0.3 with experimental data. A theoretical model was developed by Yin-Pang et al. [39], to eliminate the geometrical effect in a horizontal pipe and a correlation between void fraction and quality was chosen as a comparison.

The parabolic form of void distribution in some previous work may be assumed for symmetrical flow such as, for example, flow in a radial plane and a vertical flow bubble. A study by Yamazaki and Simizu [11] indicates the difficulty if not the impossibility of obtaining, theoretically, the profile of the void fraction and then the phase velocities on the basis of two concepts: hydrodynamic (3D-2V-1T) and hydraulic (1D-2V-2T) equations where D, V and T denote dimension, velocity and time, respectively. In the hydrodynamic equations, the nature and values of interactive forces within each phase are generally unknown. Ignorance of these terms renders the solution of the whole set of equations impossible.

The void fraction and the pressure drop, however, could either be postulated hypothetically or obtained experimentally. The number of variables in the hydraulic equations exceeds the number of equations. By omitting the interactive terms, and taking the product of density and gravitational acceleration as a constant, it can be shown that the flow is reduced to that of a hypothetical case. In this study, our main interest is the prediction of the void fraction in a large diameter, horizontal pipe with air-water mixture and highly turbulent flow. To our knowledge, little work has been done and no correlation of the void distribution has been established in this kind of flow in either longitudinal or cross-sectional planes.

PRINCIPLE OF MEASUREMENT OF THE VOID FRACTION

Definition of the void fraction

The principle of measurement of the void fraction is illustrated in Figure 1. The passage of air bubbles through a sensor placed somewhere in a pipe is revealed by electric voltages which differ from those gathered in the absence of bubbles. The use of an adjustable threshold level of a discriminator circuit makes it possible to determine the local void fraction. The void fraction determined in this way is considered as the ratio of the average travel time of the bubbles to the total measuring time, T , sufficient for the travel time of the bubbles to be

equivalent to the width of conditioned square or sinusoidal waves. These waves correspond to the passage of bubbles. The void fraction can be defined in two ways:

*Local void fraction:

$$\alpha = \frac{\sum_{i=1}^n t_{G_i}}{T} = \lim_{T \rightarrow \infty} \frac{1}{T} \int_0^T \delta(r, t, v_s) dt \quad (1)$$

where t_{G_i} is the width of the conditioned wave (front sensor of a double probe), T is the duration of measurement of the total sampling time and $\delta(r, t, v_s)$ represents phases indicative of functions corresponding to the threshold voltage V . $\delta = 0$ in the absence of bubbles and $\delta = 1$ in the presence of bubbles.

*Global void fraction:

$$\begin{aligned} - \text{Volumetric: } \bar{\alpha}_v &= \sum V_i(t)/V \quad \text{or} \quad \frac{1}{V} \int_v \alpha dV \\ - \text{Surface: } \bar{\alpha}_s &= \sum S_i(t)/S \quad \text{or} \quad \frac{1}{S} \int_s \alpha dS \\ - \text{Linear: } \bar{\alpha}_L &= \sum L_i(t)/L \quad \text{or} \quad \frac{1}{L} \int_L \alpha dL \end{aligned} \quad (2)$$

Use of hot film anemometer

Regarding the local measurement of the void fraction, each technique has certain advantages and disadvantages. For example, the laser anemometer is not used except for very weak concentrations of bubbles, and in the conductivity method, electric conductivity loses its meaning with strong concentrations of bubbles, etc.

A comparison of the optical probe, resistive probe and hot film anemometer by Galaup [12] reveals very similar results. Moujaes et al [13] and Swanand et al [46] also found that local void fractions measured using wedge type hot film anemometers were comparable to those obtained using optical fiber probes. Their experiment was performed in a large vertical rectangular channel of 12.7 x 76.2 mm cross-section. The choice of measurement method is, then, a compromise between the different parameters of interest: price, availability of measurement probes and of analysis equipment, etc. We chose the hot film anemometer method because of its widespread use in the measurement of flow velocity, intensity of turbulence, void fraction and temperature.

The output of a hot film anemometer in two-phase flow depends on the difference in heat dissipation rates during the passage of the two different phases through the probe (Hsu et al. [2], Goldschmidt and Eskinazi [14] and Delhaye [3]). The sensitivity of the hot film sensor depends on the variations of velocity in an isothermal single-phase flow and on the change of phases in a two-phase flow, the heat transfer coefficient of the liquid phase being about two to three times that of the gas phase.

The arrival of a bubble on the sensitive element causes a slow reduction in the heat transfer rate, which means less power is needed to maintain this element at a constant temperature. This power reduction is indicated by a decrease in output voltage of the hot film anemometer. The situation stabilizes as the bubble disappears and the output voltage rises rapidly. The hot film

probe is shown to be a good measuring instrument because of its rapid response to the passage of a bubble.

Fluctuating signals furnished by the hot film probe are then passed through a series of amplifiers, filters and the electrical circuit of a discriminator. Their outputs are conditioned signals which make it possible to determine the average value of the local void fraction. This value needs, however, to be compared with that obtained by a global measuring method such as quick closing valves.

EXPERIMENTAL SETUP

Calibration system

A loop is designed to perform the calibration of the hot film probe for measuring the void fraction. It consists of a series of steel and Plexiglas pipes where a continuous flow of water is delivered to the base of the vertical part of the loop. The water is supplied by a 50 HP centrifugal pump with an initial water flow rate of maximum 1600 USGPM. Compressed air at 50 psig is injected into a cylindrical mixing chamber 2.0-in. in diameter and 4.0-in in length, where a two-phase air-water flow is produced through a series of 80 1/8-in. holes pierced along the perimeter.

Water and air flow rates are maintained at a constant pressure (5 psig to 125 psig/ respectively) by a monitoring valve and a series of air filters and pressure regulators. The calibrated section consists of a clear vertical pipe 2.0 inches in internal diameter and 40 inches in length which can be closed instantaneously by means of two quick-closing valves that, when open, have the same cross section as the pipe. Hence, the valves present no restriction in the open position and the connecting parts are carefully made so as to avoid any kind of flow perturbation. An air pressure regulator of 90 psig maximum rating, called the speed control box, controls the open/close velocity of the two valves which are activated by means of a rigid mechanical connection.

In normal operating conditions, the inlet air pressure of the box is regulated at about 65 psig which corresponds to a sufficiently short response time, less than 0.5 sec. This is to avoid any irregularities which could result while the two valves are being maneuvered. Visual observations at the test section indicate that the flow is already stable at a distance of 42 times the pipe diameter from the mixing chamber. In addition, preliminary analysis of signals recorded across the pipe reveal the degree of symmetry and homogeneity of the flow.

Air and water temperatures are measured by means of regular thermometers. After passing through the flow circuit, the mixture is collected in a separating tank, where the water is sent back to the pump while air bubbles escape freely into the surrounding atmosphere.

Experimental system

Experiments were performed in a horizontal closed loop which has been described by Lakis et al. [15]. A large horizontal flow circuit is fed by one centrifugal pump of 150 HP and two centrifugal pumps of 75 HP each. This pumping system feeds the loop at a rate of 2000 to 5000 USGPM from a 15000 USG reservoir. Water flow rates are regulated as it passes through a closed 2500 USG pressure vessel, and then through a mixer of 2000 holes 3.0 mm in diameter where compressed air is injected to produce a two-phase flow.

This mixture finally runs through a horizontal pipe 130 diameters in length and returns to the open reservoir. The experimental section consists of a series of PVC, steel and Plexiglas pipes of 8.0-in nominal diameter, schedule 80. Water and air flow rates are controlled by means of calibrated orifice flow meters which are connected respectively to their differential Hg and H₂O manometers. Temperatures of air and water are indicated by well-protected thermometers placed at the entrance to the mixer and near the loop exits.

Several pressure taps placed along the pipe permit measurement of the pressure drop. In addition, 3 equidistant holes 10/32 in. in diameter were made around one-half of the pipe perimeters, from the top to the bottom. Piezometric lines are essential for controlling the stability and reproducibility of the measurement conditions in both single and two-phase flows. Finally, a central line was drawn at each axial measurement location (top side of the pipe) to facilitate the alignment of the probe. This alignment ensures that the axial direction of the sensor placed in the pipe is parallel to that of the pipe and hence the flow. The up and down motion of the sensor's support is controlled by means of a traverse mechanism.

Experimental conditions

Flow patterns depend fundamentally on the initial flow rates or the superficial velocity of each constituent phase. Several investigators have proposed a variety of flow maps corresponding to specific flows. There are graphic representations in different forms where flow patterns may be identified by superficial velocities (Govier and Omer [16], Taitel and Duckler [17], Mandhane et al. [18], Sekoguchi et al. [19], Barnes et al. [20], by ratio of volumetric flow rate to Froude number (Golan and Stenning [21]), or by energy spectrum of phases (Hubbard and Ducker [22], Hewitt and Roberts [23], Chisholm, etc.).

According to Savery [25], flow patterns in air-water horizontal flows with liquid predominating, vary widely and depend on the given initial flow rate of the continuous phase. Also, measurements carried out in two different horizontal pipes, 2.54 and 9.53 cm in diameter ([26]) indicate the complexity of the transition mechanism for the same flow conditions. In this study, visual observations of flow patterns agree more or less with those of Mandhane et al. [18] and Hoogendoorn [27] which are the easiest to compare. However, the choice of flow rate volumetric quality, X_0 (ratio of gas volumetric flow to total volumetric flow rate) for current experimental work is limited by loop capacity. Practical applications demand more accurate flow identification. For this purpose, selected experimental conditions are given in Table 1, and observed flow patterns are illustrated in Figure 3.

Hot film probe and its support

A double conical hot film probe was designed to measure simultaneously a pair of passing bubble signals. The first signal, given by the front sensor, provides void fraction information. Both front and rear signals are used to determine the local linear velocity of the bubbles. The choice of a conical form has the advantage of preventing the sensor from being deformed or broken by deposits of impurities, particles or filaments in suspension in the water. It also prevents fatigue failure due to excessive vibration produced by vortex shedding, such as occurs with a cylindrical probe. The probe consists of two very thin films of platinum and a thin dielectric layer. The thickness of the films is nearly 0.1-in. With providing the fissuration of platinum films and with their quartz coating, the films have been designed to be stable, i.e.

without resistance variation in cold temperatures. In addition, they are resistant to contamination or erosion.

The separation distance d between two films is estimated by using cinematography to determine the mean diameter of air bubbles d_G at the clear test section. Optimum values of d and d_G are 3.03 mm and 2 to 3mm. respectively. The probe was made by TSI Company and is shown in Figures 4 and 5. Its rigid support may be positioned accurately in the flow. It comprises:

- A helicoidally endless screw displacement mechanism.
- A vertical adjustable scale for compensating for the number of threads in the pipe orifice once the probe has been screwed in.
- Two big screws of the clamp type for attenuating the vibration of the probe support, especially when the probe is in the lower part of the pipe and when the flow rate is high.
- A directional indicator to ensure that the direction of the sensor placed in the pipe and that of the flow are the same.

Calibration procedure

The calibration procedure includes calibration of the hot film sensor in both single-phase and two-phase water flow, calibration of the magnetic recorder and the electric circuit of the discriminator, and verification of related accessories.

Calibration of hot film in water flow

A hot film anemometer can be operated in two ways:

1. At constant intensity: measure film resistance at a constant current.
2. At constant temperature: measure necessary current to maintain constant temperature of film, hence its resistance.

The former is rarely used owing to complications introduced by the necessity for compensating for the resulting variations of heat exchange between the sensitive element and its support (Resch and Coantic [28], Bouvard and Dumas [29]). In order to limit the temperature of the sensitive element to the lowest possible value but still give satisfactory sensitivity, the overheat ratio corresponding to the film in water at 80 °C was calculated to be equal to about 1.1. Calibration of the hot film in water is schematically shown in Figure 6. Conditions in which two different models of hot film were calibrated are also given in Table 2. The calibration procedure may be summarized as follows:

- Disconnect the probe from the cable ($\approx 5\text{m}$) and replace it with a shorting probe, balance the bridge with a potentiometer until its resistance is zero ($R=0$).
- Dip the cold probe in static water (in fact with a continuous current of very low flow rate in order to avoid the formation of bubbles on the heated element, and to maintain the water temperature at $T^{\circ} \text{ amb} \pm 0.05^{\circ} \text{ C}$). Rebalance the bridge with the probe resistance.
- Multiply this value by the calculated overheat ratio. The result represents the operating resistance of the hot film.
- Start the servo amplifier and obtain output voltage by means of a voltmeter.

Morrow [30] demonstrated experimentally that, in spite of an advantageous geometry, the accumulation of impurities at the film surface might reduce the heat transfer rate. Therefore, the output voltage may possibly not be uniquely a function of velocity or the temperature of

the fluid. For this reason, the probe is carefully cleaned with alcohol and distilled water before and after use.

According to Davies and Patrick [31], for high Reynolds numbers ($>10^5$), the output voltage of the anemometer, the sensitivity of the film and the intensity of turbulence may be expressed as:

$$\text{- Output voltage: } E^2 = A + BU^{\frac{1}{2}} + CU \quad (3)$$

$$\text{- Sensitivity of film: } \frac{dE}{dU} = \frac{BU^{-\frac{1}{2}} + 2C}{4E} \quad (4)$$

$$\text{- Intensity of turbulence: } \frac{\sqrt{u}}{U} = \frac{8CE\sqrt{E'^2}}{B^2 + 4C(E^2 - A) - B(B^2 - 4C(E^2 - A))^{\frac{1}{2}}} \quad (5)$$

where E : average output voltage (volt DC), E' : fluctuating component of E (RMS), U : average flow velocity, u : fluctuating component of U and A , B , C : unknown constants.

With the results of (3), (4) and (5), the calibration curve of the front film of probe, model 1231 AF W, was plotted and is given as an example in Figure 7. The dynamic sensitivity of the hot film and the intensity of longitudinal turbulence are also given in Table 3.

Calibration of hot film in two-phase flow

This step is carried out in the vertical calibration loop for the simple reason that the determination of the void fraction by quick closing valves in the large 8-in. diameter test pipe is impractical because of unacceptable flow disturbances generated by the undersize values. Calibration of hot film in two-phase flow is schematically shown in Figure 8. Details of the calibration procedure are also illustrated in Figure 9. Signals delivered by the front film of a conical double probe pass through a discriminator circuit, the output of which is a square wave of equivalent height to that of an adjustable threshold (Fig. 8).

The maximum threshold height corresponds to 1 V for the output signal readjusted to 2 V peak to peak from the recorder. A time counter connected to the output of the circuit provides the sum of square waves in seconds or milliseconds. The ratio of this sum to total sampling time is equivalent to the average local void fraction. The number of square waves measured by a frequency meter during a given sampling time represents the bubble impact rate. Apparatus and experimental conditions are almost the same in both calibration and test phases. Amplification and attenuation of recorded signals were achieved with Ithaco 451 amplifiers and a Hewlett Packard 350D attenuator.

The discriminator circuit was constructed and tested with square and sinusoidal waves of various known frequencies. For calibration and measurement for a given sample, the total time was measured by a chronometer. The average absolute errors in the determination of wave width and number of waves in the range of <2.5 kHz were 0.3 % and 0.1 %, respectively, where:

$$\text{Absolute Error} = \frac{1}{n} \sum \left| \frac{\alpha_{\text{known}} - \alpha_{\text{mes.}}}{\alpha_{\text{known}}} \right| * 100$$

Choice of optimum threshold

Referring to Figure 9, when each signal $V(t)$ obtained at a given radial position passes through the discriminator, for each value V_D of interest that one can choose from an adjustable voltage level of the threshold, the corresponding output at the time meter during a sampling time T is the sum $(\sum_{i=1}^m t_{Gi})_{Dj}$. Repeating the same procedure with various values of voltage level V_D , a graph indicating the variation of T with V can be drawn. The function in the graph may be divided approximately into two parts: A (liquid dominated) and B (gas important). Part A is established when the threshold is found in the zone dominated by the gas phase. A zero value of $\sum_{i=1}^m t_{Gi}$ indicates that no bubble signal has been detected at the threshold; this is normally the starting point of the function. Part B is established when the threshold moves up slowly near the liquid voltage level, and represents the peaks which result not only from the passage of bubbles, but also from the fluctuation of the liquid phase itself and supplementary fluctuation due to bubble agitation.

The degree of perturbation varies within flow patterns and from one radial position to another. The critical point between parts A and B is judged by visually examining the signals with a special oscilloscope. The judgement is based on whether or not there is a significant change in $\sum_{i=1}^m t_{Gi}$ (as indicated by the time counter) between two successive values of V_D , for the same small increment. In repeating the same procedure for various radial positions, various values of α_{ind} will be obtained where:

$$\alpha_{ind} = \frac{\left[\sum_{i=1}^m t_{Gi} \right]_{Dj}}{T} \quad (6)$$

α_{ind} represents the local void fraction determined by the hot film technique (indirect method). Correction will be made by comparison with the void fraction obtained by the global or direct method.

By performing the numerical integration of all α_{ind} evaluated for one value of flow volumetric quality, X_0 , on the volume of the pipe (tube of calibration loop), I_1 can be obtained. If the flow is homogeneous and the distribution of α_{ind} is uniform at all points in the volume, the equality $I_1 = \alpha_{ind}$ indicates that the choice of threshold level is correct.

Evaluation of signals indicates that the bubbles are spread in a symmetrical way and are almost uniform in the calibration section.

Global method

This method consists of measuring instantaneously the volume of water in an air-water flow mixture at a given moment in time and deducing the volume of air. The result represents the volumetric void fraction. The volumes of water contained in the tube before and after quickly closing the valves may be defined as:

$$\begin{aligned} \text{- Initial:} \quad & V_{Li} = \frac{m_{LSi} - m_s}{\rho_L} \\ \text{- Final:} \quad & V_{Lf} = \frac{m_{LSf} - m_s}{\rho_L} \end{aligned}$$

where m_s mass of empty container (606.9 gr), m_{LSi} : mass of container and initial liquid (valves in open position)(3075 gr.), m_{LSf} : mass of container and final liquid (after closing two valves) and ρ_L : density of water.

If α_v is the ratio of final air volume found in the tube to total volume of water in the fully filled tube, we must have:

$$1 - \alpha_v = \frac{V_{Lf}}{V_{Li}}$$

$$\text{with} \quad \alpha_v = \frac{m_{LSi} - m_{LSf}}{m_{LSi} - m_s} \quad (7)$$

$$\text{or} \quad \alpha_v = 4.052 * 10^{-4} (3075 - m_{LSf}) \quad (8)$$

In practice, the volumetric void fraction, α_{dir} , is obtained by taking the average value of some α_v . The reproducibility of results depends on the response of the closing mechanism; two to three values of α_v are reasonable in general. The time taken for the flow to stabilize after each closure is about 15 minutes.

Figure 10 shows the calibration curve for the void fraction. A linear relationship was found to exist between void fractions measured by quick closing valves and those measured by hot film.

Figure 11 illustrates an example of a void fraction determined by the hot film probe & discriminator technique over a period of 160 sec. Some other examples of the determination of void fractions in a large pipe (horizontal test loop) are also given in Figure 12, where tests were carried out at various flow volumetric qualities, X_0 , and with axial location, z/D .

In a large pipe, the choice of threshold level is delicate for measurements near the upper pipe wall because of very strong fluctuation (vortex of flow may exist in the space of the pipe orifice when the probe is not precisely placed along the height of this orifice) and several samples and a detailed examination of signals are required; measuring time is normally 4 to 5 times longer than that at positions far from the upper wall in order to be able to base judgement on an average value. The difference in reproducibility of measurement taken under the same experimental conditions but at different moments is 10 to 15% for positions near the upper wall and about 10% for others.

RESULTS AND PROPOSED CORRELATIONS

Experiments were carried out at the pipe center line along 24 equidistant axial locations on a total length from the mixer of 130 times the pipe diameter. Local void fraction distributions were obtained by measuring over both transversal and radial planes at each axial location, where 9 radial positions were defined for each cross-sectional plane. In order to verify the

reproducibility of results, all local measurements were repeated at least 3 times under the same experimental conditions.

Longitudinal distribution of void fraction

The variation of measured void fraction at the center line of the pipe along the axis, performed for different flow volumetric qualities, X_0 , is given in Figure 13.a. Examples of void fraction profiles taken at the clear working sections downstream and at highest water flow rate can be seen in Figure 13.b. It can be seen that there is a change in the void fraction profile when $X > 0.116$; in terms of axial location $z/D=92; 130$ and 150 . There is also a complete change in the void fraction profile with increases in X_0 . Visual observations of flow also indicate that there is a great accumulation of bubbles in the upper half of the pipe and a relatively small one in the lower part.

It may be said that the flow perturbations originating at a sufficiently high air flow rate from the exits of the mixer provide a test of the downstream section. They greatly influence the void fraction profile which in turn influences the profile of other flow parameters. The longitudinal distribution of the void fraction also indicates that the void fraction is a function both of volumetric quality, X_0 , and axial location, z/D . In normalizing the measured void fraction at the pipe center line at different axial locations, α , with respect to those at the pipe center line of fully developed flow, α_{FD} , ($z/D > 130$), the longitudinal distribution of the void fraction may be assumed to be :

$$\frac{\alpha_{CL}}{\alpha_{FD}} = A(z/D) + B \quad (9)$$

where α_{CL} : measured void fraction at the pipe center line of each axial location z/D

α_{FD} : measured void fraction at the pipe center line of fully developed flow, $z/D > 130$

z : Pipe length measured from mixer

D : Nominal diameter of pipe

A, B : Unknown constants.

Furthermore, constants A and B may be expressed in terms of flow volumetric quality, X_0 , as follows:

$$A = A_1 X_0 + A_2$$

$$B = B_1 X_0 + B_2$$

where $X_0 = \frac{\text{initial air volumetric flow rate}}{\text{initial "air + liquid" volumetric flow rate}}$,

A_1, A_2, B_1, B_2 : Unknown constants. Constants A_1, A_2, B_1 and B_2 are finally determined by linear regression where (9) can be written as (Fig. 14):

$$\frac{\alpha}{\alpha_{FD}} = -(0.009X_0 - 0.015)(z/D) + (-1.88 X_0 + 2.03) \quad (10)$$

Cross-sectional distribution of the void fraction

In order to obtain a true image of the void fraction profile in a large diameter horizontal pipe, measurements were performed through 9 radial positions in each cross-sectional plane. At the highest flow rate of, for example, water measurements in the lower part of the pipe were sometimes achieved separately after experiments in the upper part had been completed. The probe placed in the pipe flow may be considered as a clamped, free beam in a vibration field. Vibration of the probe itself could interfere with the data collection and easily damage the sensor.

The rigidity of the probe traversing mechanism and that of the sensor support, the existence of particles in suspension, the direction of the sensor in the flow and any source of vibration require a great deal of attention during experimentation.

Transversal plane

Void fraction profiles in the transversal plane measured at axial location $z/D = 130$ are given in Figures 15.a. Functional dependence of the void profile in the transversal planes expressed in terms of flow volumetric quality, X_0 , and axial location, z/D , is shown in Figure 16.a and 16.b, respectively. Variation of the local void fraction with flow volumetric quality, X_0 , is also examined at different radial positions in the transversal planes; the results for three axial locations downstream are given in Figure 16.c.

Through them, the non-uniformity of the profiles, brought about by phase separation, indicates that the curves represent neither a parabolic nor a power law distribution. As it is not always easy to obtain reliable measurements in the vicinity of the pipe wall, values at the wall may be postulated such that correlations may be made relatively simply. In other words, the prediction models will be valid for measurements carried out in the range of $0.555 < y/D < 0.945$, where y/D is the normalized distance measured from the upper part of the pipe.

Furthermore, most of the water is in the lower part of the pipe where air bubbles are practically non-existent, as previously indicated by visual observation of flow even at nearly 30% maximum flow volumetric quality. The void fraction can then be considered as having a zero value at the lower wall ($y/D=1$). In the upper part of the pipe ($y/D=0$) where air bubbles are normally concentrated, the void fraction is assumed to be zero although it probably has certain non-zero values. After several attempts, it was found that the distribution of the void fraction in the transversal plane may be predicted by postulating the following two models:

* **Model 1:** The void profile is approximated by linear functions such as:

The constants A_1 , A_2 , B_1 and B_2 are determined by linear regression where, (Figure 17):

$$\begin{aligned}\alpha &= A_1(y/D) + B_1 \quad (0.0 \leq y/D \leq 0.6) \\ \alpha &= A_2(y/D) + B_2 \quad (0.6 \leq y/D \leq 1.0)\end{aligned}\quad (11)$$

$$\begin{aligned}\alpha &= -1.361(y/D) + 2.734 \quad (0.0 \leq y/D \leq 0.6) \\ \alpha &= -3.333(y/D) + 1.594 \quad (0.6 \leq y/D \leq 1.0)\end{aligned}\quad (12)$$

This model gives the non-zero values at the pipe wall.

***Model 2**: Using the assumption of zero values of the void fraction at the pipe walls, the void profile is assumed to be the product of power and exponential functions, such as:

$$\alpha = (y^{*a} - y^*)e^{-by^*} \quad (13)$$

where $y^* = y/D$: normalized distance measured from wall; a and b are unknown constants.

Constants a and b determined by regression are: $b = 1$ and $a = e^{-8.46X_0}$ (Figure 18).

A comparison of the values predicted by the two models and experimental results is shown in Figure 19, where:

	Arithmetic mean deviation	Standard deviation
Model 1	1.7 %	3.5 %
Model 2	4 %	3.3 %

Radial plane

Measurements of the void fraction in the radial plane are carried out in the same way as those in the transversal plane. An example of void profiles measured in fully developed flow ($z/D = 110$ and 130) at various flow volumetric qualities, X_0 is given in Figure 15.b. Theoretically, gravity has no effect on the variation of flow parameters or phase separation in this plane. The profiles are, therefore, symmetrical and resemble those of most vertical flows.

The void fractions are distributed almost uniformly through the cross-section of the pipe. However, the profile appears to become concave as flow volumetric quality, X_0 increases. This implies that the given flow would probably be annularly dispersed in a moment with a strong concentration of air bubbles along the pipe perimeter. Values of the void fraction in this plane are found to be nearly equal to those near the pipe axis.

Because the form of the profiles is similar to that of the velocity distribution in turbulent water flow, the power law may be assumed for the distribution of the void fraction in a radial plane where:

$$\frac{\alpha}{\alpha_{CL}} = a(1 - |2y^* - 1|)^b \quad (14)$$

where α : local void fraction

α_{CL} : Measured void at pipe axis

$y^* = y/D$: Normalized distance measured from wall

a and b are unknown constants.

Similarly, regression analysis gives finally

$$\frac{\alpha}{\alpha_{CL}} = 1.0 (1 - |2y^* - 1|)^{0.011} \quad (15)$$

A comparison of the predicted values obtained by (15) and experimental results is shown in Figure 20 (arithmetic mean deviation = 0.5 %, standard deviation = 1.5 %). In both transversal and radial planes, the void fraction profiles are qualitatively comparable with those obtained numerically by Brown and Kranich [9] in a linear pipe with $Re = 175,000$.

CONCLUSION

The distribution of the void fraction was investigated in the axial direction and in cross-sectional planes of a pipe with the help of a hot film anemometer. The use of a hot film with a discriminator circuit has been shown to be a good technique for determining the local void

fraction in small diameter pipes. However, its indicative values need to be compared with those obtained by a global method if we are to achieve a satisfactory definition of the void fraction.

A vertical calibration loop was constructed to calibrate the hot film in a symmetrical bubble flow. The calibration curve indicates a linear relationship between void fractions determined by the hot film method and those obtained by the quick-closing valves method. This curve, which is valid only for the one hot film under consideration, is used to obtain the values measured by the hot film in large diameter pipes.

Experimentation in a horizontal test loop indicates that difficulty sometimes arises in the choice of an optimum threshold level, especially in dealing with signals recorded in the near wall region (< 1 in. from wall in an 8 in pipe). An average value of the threshold was taken after 6 measurements which were considered reasonable. Outside this region, the fluctuation of the signal due to the passage of air bubbles is more obvious and the threshold can easily be determined.

New correlations were proposed to predict the distribution of the void fraction in the longitudinal and both cross-sectional planes of the pipe. In the longitudinal direction, the void fraction can be linearly expressed in terms of axial location and flow volumetric quality. In the radial plane, the void fraction profiles are symmetric and similar to those of vertical flow, the power law being perfectly applied in this case. In the transversal plane, the profiles are asymmetric and in turn affect the phase distribution and mixture velocities. Void fraction distribution in this plane may be predicted either by a linear model or by a power time's exponential model. It was also found that the profiles are qualitatively similar to those obtained in a small diameter pipe with horizontal flow. The effect of gravity on phase separation is greater than that of turbulent bubble diffusion in the transversal plane.

Nomenclature

- D Pipe diameter
- E Average output voltage (Volt DC)
- E' Fluctuating component of output voltage (RMS)
- m_s Mass of empty container
- m_{L_i} Initial mass of liquid alone contained in fully filled tube
- $m_{L_s i}$ Initial mass of container fully filled with liquid
- m_{L_f} Final mass of liquid in tube after quickly closing the valves
- T Total sampling time
- t_{G_i} Width of conditioned wave of front sensor
- U Average flow velocity
- u Fluctuating component of average flow velocity
- V Volume
- X_0 Flow volumetric quality (ratio of initial air flow rate to initial total flow rate)
- v Transversal direction
- z Axial of longitudinal direction
- α Local void fraction
- α_{CL} Measured void fraction at pipe center line of each axial location z/D

- α_{FD} Measured void fraction at pipe center line of fully developed flow,
 $z/D > 130$.
- α Ratio of air volume in tube to total volume of water in fully-filled tube.
- $\delta(r, t, v)$ Phase indicative function corresponding to threshold level V
- ρ_L Density of water

REFERENCES

- [1] NEAL, L.G., BANKOFF, S.G., "A High Resolution Resistive Probe in Gas-Liquid Flow", *AICHE, J.*, Vol. 9, 490-494, 1963.
- [2] HSU, Y.Y., SUMON, F.F., GRAHAM, R.Q., "Application of Hot Wire Anemometry for Two-Phase Flow Measurements such as Void Fraction and Slip Velocity", Prepared for ASME Winter Meeting, Philadelphia, 17-22, Nov. 1963.
- [3] DELHAYE, J. M., "Anémomètre à film cc ud dans les écoulement diphasiques. Mesure du taux de présence du gaz", *C.R. Acad. Sc. Paris*, t.266, série A, 370-373, février 1968.
- [4] KAZIN, I.V., "Radial distribution of Vapor in Upward Turbulent Steam Water Flow", *Teploenergetika*, Vol. 1, 40-43, 1964.
- [5] MILLER, N., METCHIE, R.E., "The Development of a Universal Probe for Measurement of Local Voidage in Liquide/Gaz Two-Phase Instrumentation", *Proc. 11th Nat. ASME/AICHE Heat Transfer Conf. on Two-Phase instr.*, Minneapolis, Minnesota, 82-88, 1969.
- [6] OHBA, K., KISHIMOTO, I., OGASAWARA, M., "Simultaneous Measurement of Local Liquid Velocity and Void Fraction in Bubbly Flows Using a Gas Laser-Part II. Local Properties of Turbulent Bubbly Flow", *Technol. Rep. Osaka Univ.*, Vol. 27, No. 1358, 228-238, Mars 1977.
- [7] BROWN, R.W., GOMEZPLATA, A., PRICE, J. D., "A Model to Predict Void Fraction in Two-Phase Flow", *Chemical Engineering Science*, Vol. 24, 1483-1489, 1969.
- [8] ZIVI, S. M., "Estimation of Steady State Steam Void Fraction by Means of the Principle of Minimum Entropy Production", *J. of Heat Transfer, Trans. ASME, Serie C*, Vol. 86, 247-252, May 1964.
- [9] BROWN, F. C., KRANICH, W. L., "A Model for the Prediction of Velocity and Void Fraction Profiles in Two-Phase Flow", *AICHE J.*, Vol. 14, 750-758, September 1968.
- [10] WANG, S. K., LEE, S. J., JONES Jr, O. C., and LAHEY Jr, R. T., "3-D Turbulence Structure and Phase Distribution Measurements in Bubbly Two-Phase Flows", *Int. J. Multiphase Flow*, Vol. 13, No. 3, 327-343, 1987.
- [11] YAMAZAKI, Y., SIMUZU, M., "Hydrodynamic and Hydraulic Studies on Void Fractions in Two-Phase Flow", *J. of Nuclear Science and Technology*, Vol. 15, No. 12, 886-898, December 1978.
- [12] GALAUP, J. P. "Contribution à l'étude des méthodes de mesure en écoulement diphasique", *Thèse de Doctorat, Université de Grenoble* 1975.
- [13] MOUJAES, S., DOUGALL, R.S., "Experimental Investigation of Concurrent Two-Phase Flow in a Vertical Rectangular Channel". *The Canadian J. of Chem. Eng.*, Vol. 65, 705, October 1987.
- [14] GOLDSCHMIDT, V., ESKINAZI, S., "Two-Phase Turbulent Flow in a Plan Jet", *J. of Applied Mechanics*, Vol. 33, No. 4, 735- 747, 1966.
- [15] LAKIS, A. A., MOHAMED, S. S., ROUSSELET, J., "Turbulent Two-Phase Flow Loop Facility for Predicting Wall-Pressure Fluctuations and Shell Response", 24th

- International Instrumentation Symposium, May 1-5, 1978, Albuquerque, New Mexico, Instrument Society of America (ISA), p. 267-274.
- [16] GOVIER, G. W., OMER, M. M., "The Horizontal Pipeline Flow of Air-Water Mixtures", the Canadian J. of Chemical Eng., 93-104, June 1962.
- [17] TAITEL, Y., DUCKLER, A. E., "A Model for Predicting Flow Regime Transitions in Horizontal and Near-Horizontal Gas-Liquid Flow", AICHE J., Vol 22, 47-55, 1976.
- [18] MANDHANE, J. M., GREGORY, G.A., AZIK, K.A., "A Flow Pattern Map for Gas-Liquid Flow in Horizontal Pipes", Int. J. Multiphase Flow, Vol. 1, 537-553, 1974.
- [19] SEKOGUCHI, T., AKAGAWA, K., HAMAGUCHI, H., IMOTO, M., ISHIDA, S., "Flow Regime Maps for Developing Steady Air-Water Two-Phase Flow in Horizontal Tubes", Mem. Fac. Eng. Kobe Univ., Vol. 25, 191-202, 1979.
- [20] BARNES, D., SHOHAN, O., TAITEL, Y., DUCKLER, A. E., "Flow Pattern Transition for Horizontal and Inclined Pipes: Experimental and Comparison with Theory", Int. J. of Multiphase Flow, Vol. 6, 217-225, 1980.
- [21] GOLAN, L. P., STENNING, A. H., "Two-Phase Vertical Flow Maps", Prod. Instn. Mech. Engrs., Vol. 184, Part 3C, 108-114, 1969-1970.
- [22] HUBBARD, M. G., DUCKLER, A. E., "The Characterization of Flow Regimes for Horizontal Two-Phase Flow", Proc. of the 1966 Heat Transf. and Fluid Mech. Inst., Stanford, 100-121, 1966.
- [23] HEWITT, G. F., ROBERTS, D. N., "Studies of Two-Phase Flow Patterns by Simultaneous X-Ray and Flash Photography", A. E. R. E., M. 2159, 1969.
- [24] CHISHOLM, D., "Flow Pattern Maps in Horizontal Two-Phase Flow", Int. Conf. on the Physical Modeling of Multiphase Flow, Coventry, Great Britain; Communication F1, 219-232, 19-21 April 1983.
- [25] SAVERY, C. W., "Flow Patterns in Two-Phase Flow". The Symp. on Polyphase Flow and Transport Technology, Century 2 Emerging Technology Conf., San Francisco, CA., ASME, 75-88, 13-15 August 1980.
- [26] LIN, P. Y., HANRATTY, T. J., "Effect of Pipe Diameter on Flow Patterns for Air-Water Flow in Horizontal Pipes", Int. J. Multiphase Flow, Vol .13, No. 4, 549-563, 1987.
- [27] HOOGENDOORN, C. J., "Gas-Liquid Flow in Horizontal Pipes", Canadian J. of Chemical Eng. Sci. , Vol. 9, 205-217, 1959.
- [28] RESCH, F., COANTIC, M., "Étude sur le fil chaud et le film chaud dans l'eau ", La Houille Blanche, No. 2, 151-161, 1969.
- [29] BOUVARD, M., DUMAS, J. "Application de la méthode de fil chaud à la mesure de la turbulence dans l'eau", La Houille Blanche, No. 3, 257-270, No 7, 723-734, 1967.
- [30] MORROW, T. B., "Effects of Dirt Accumulation on Hot Wire and Hot Film Sensors", Fluid Dynamic Measurement: Discussion-Conference Papers, Vol. 1, 122-124, 1972.
- [31] DAVIES, T. W., PATRICK, M. A., "A Simplified Method of Improving the Accuracy of Hot Wire Anemometry", Third Dynamic Measurement Conference Papers, Vol.1, 152-155, 1972.
- [32] TEYSSEDOU, A., AUBE, F., CHAMPAGNE, P., "Void fraction measurement system for high temperature flows", Measurement Science and Technology, vol. 3, 485-494, 1992.
- [33] THIYAGARAJAN, T. K., DIXIT, N. S., SATYAMURTHY, P., "Gamma-ray attenuation method for void fraction measurement in fluctuating two-phase liquid metal flows", Measurement Science and technology, vol.2, 69-74, 1991.
- [34] JIANG, Y., REZKALLAH, K.S., "An experimental study of the suitability of using a gamma densitometer for void fraction measurements in gas-liquid flow in a small diameter tube", Measurement Science and Technology, vol. 4, 496-505, 1993.

- [35] CARTELLIER, A., “Optical probes for local void fraction measurements: characterization of performance”, *Review of Scientific Instruments*, vol. 61, 874-886, 1990.
- [36] MORRIS, D., TEYSSEDOU, A., LAPIERRE, J., “Optical fiber probe to measure local void fraction profiles”, *Applied Optics*, Vol. 26, 4660-4664, 1987.
- [37] SERDULA, C.D., LOEWEN, M.R., “Experiments investigating the use of fiber-optic probes for measuring bubble-size distributions”, *IEE-Journal of Oceanic Engineering*, vol. 23, 385-399, 1998.
- [38] TEYSSEDOU, A., TAPUCU, A., LORTIE, M., “Impedance probe to measure local void fraction profiles”, *Review of Scientific Instruments*, vol. 59, 631-638, 1988.
- [39] YIN-PANG, MA., NIEN-MLEN, C., BAU-SHEI, P., WEI-KENG, L., YIN-YUN, H., “Two simplified methods to determine void fractions for two-phase flow”, *Nuclear Technology*, Vol. 94, Iss :1, 124-133, 1991.
- [40] ELKOW, K.J., REZKALLAH, K.S., “Void fraction measurements in gas-liquid flows using capacitance sensors”, *Measurement Science and Technology*, vol. 7, 1153-1163, 1996.
- [41] GUPTA, S., DAS, P. K., “Finite-Difference resistance modeling for liquid level measurement in stratified gas-liquid systems”, vol. 5, 574- 579, 1994.
- [42] CHIEN, K.H., LIN, W.K., TSAI, Y.C., “An effect of the side-tube configuration on the void fraction measurement”, *Nuclear Technology*, Vol. 120, 171-178, 1997.
- [43] Melkamu A. Woldesemayat, Afshin J. Ghajar. Comparison of void fraction correlations for different flow patterns in horizontal and upward inclined pipes. School of Mechanical and Aerospace Engineering, Oklahoma State University, Stillwater, OK 74078, USA. *International Journal of Multiphase Flow* 33 (2007) 347–370.
- [44] Bhagwat, Swanand M; Ghajar, Afshin J. Similarities and differences in the flow patterns and void fraction in vertical upward and downward two phase flow. *Experimental Thermal and Fluid Science*, 05/2012, Volume 39.
- [45] Thome, John R; Cioncolini, Andrea. Void Fraction Prediction in Annular Two-Phase Flow Using an Algebraic Turbulence Model. *Microgravity Science and Technology*, 09/2010, Volume 22, Numéro 3.
- [46] Swanand M. Bhagwat, J. G Afshin. A flow pattern independent drift flux model based void fraction correlation for a wide range of gas–liquid two phase flow. *International Journal of Multiphase Flow* 59 (2014) 186–205.

List of Tables

Table 1: Experimental conditions.

Table 2: Calibrating conditions of hot film in water flow.

Table 3: Sensitivity of hot film and intensity of turbulence ($A=0.04$, $B=1.76$, $C=0.12$ procedure of [30]).

List of Figures

Figure 1: Local void fraction determined by discriminator technique with conditioned square waves.

Figure 2: Horizontal test loop.

Figure 3: Flow map of horizontal air-water flow. (8-in nominal diameter, fully developed flow $z/D=130$).

Figure 4: Model TSI 1231 AF-W (separation distance=1.14 mm).

Figure 5: Model TSI 1231 AM-W (separation distance=3.30 mm).

Figure 6: Calibration of hot film in water flow.

Figure 7: Calibration curve of the hot film 1231 AF-W (front sensor).

Figure 8: Schematic diagram of calibration of hot film in air-water flow.

Figure 9: Calibration procedure of hot film for determining void fraction.

Figure 10: Calibration curve for void fraction (void by quick closing values=1.426 * void by hot film).

Figure 11: Illustration of void fraction determination with optimum threshold ($z/D=74$, $y/D=0.5$, $X=0.219$, @0.610 V DC, void=0.163).

Figure 12: Average duration of bubbles obtained at optimum value of threshold level Optimum void = $\sum t_G / T$ (front sensor).

Figure 13: Longitudinal distribution of void fraction for different flow volumetric quality, X_0

- a. Void fraction measured at pipe center line
- b. Void fraction profiles in transversal plane of fully developed flow ($Q_{L_0} = 4373$ USGPM, 1: $X = 0.116$, 2, $X = 0.264$).

Figure 14: Longitudinal distribution of void center line / void fully developed flow.

Figure 15: a. Void fraction profiles in transversal plane (see table 1), $Z/D=130$

b. Void fraction profiles in radial plane (see table 2), $Z/D=130$.

Figure 16: a. Variation of void fraction profiles in transversal plane and in terms of various flow volumetric qualities X_0 , Comparison made at 3 axial locations

b. Variation of void fraction profiles in transversal plane and in terms of various axial locations z/D , comparison made for 3 values of flow volumetric quality X

c. Variation of local void fraction in terms of radial position y/D in the transversal plane, for various flow volumetric qualities and axial location.

Figure 17: Variation of constants A_1, B_1, A_2 and B_2 in linear model of void fraction in terms of flow volumetric quality X_0 .

Figure 18: Variation of exponent "a" in power & exponential model of void fraction in terms of flow volumetric quality X_0 .

Figure 19: Comparison between experimental results and proposed void fraction correlations in transversal plane (a: linear model, b: power & exponential model).

Figure 20: Comparison between experimental results and proposed void fraction correlation in radial plane.

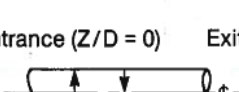
AIR			WATER		
$T_G = 24^\circ \pm 2^\circ\text{C}, P_G = 50 \text{ PSIG}, \rho_G = 0.255 \text{ lbm/ft}^3$			$T_L = 19^\circ \pm 2^\circ\text{C}, P_L = 1 \text{ ATM}, \rho_L = 62.4 \text{ lbm/ft}^3$ $\nu_L = 1.088 \times 10^{-5} \text{ ft}^2/\text{sec}$		
$Q_{Go}(\text{ft}^3/\text{min})$	$U_{Go}(\text{ft}/\text{sec})$	X_o	$Q_{Lo}(\text{USGPM})$	$U_{Lo}(\text{ft}/\text{sec})$	
76.6	4.03	.116	4373	30.74	
73.8	3.88	.131	3666	25.77	
147.6	7.76	.219	3940	27.69	
209.8	11.03	.264	4373	30.74	
202.2	10.63	.292	3666	25.77	
$X_o = \frac{Q_{Go}}{Q_{Go} + Q_{Lo}}, Q_{Go} = 19.02 * U_{Go}, Q_{Lo} = 142.26 * U_{Lo}, \rho_G = \frac{2.698 * (\text{PSIG})}{459.69 + ^\circ\text{F}}$					
$ID = 7.625 \text{ in}, Re_L(\text{max}) = 2 * 10^6, Mach(\text{max}) = 0.014 (< 0.2, \text{incompressible})$					
Entrance (Z/D = 0)			Exit (Z/D = 170)		
					
			* 24 Axial locations		
			* 9 Radial positions (Transversal plane A and Radial plane B)		

Table 1: Experimental conditions.

Probes	Position	$T_{AMB}(c^\circ)$ Ω	$T_{Water}(c^\circ)$	$R_{Water}(\Omega)$	$R_o(\Omega)$	$T_{3C}(c^\circ)$	$r(\Omega)$	$C_s/(c^\circ)$
1231 AK-W	Front	22.0 10^{-3}	18.3 5.17	4.78	5.05	66.7	0.12	2.25*
	Rear	22.0 10^{-3}	18.3 4.69	4.37	4.58	66.7	0.12	2.13*
1231 AM-W	Front	20.0 10^{-3}	17.5 8.39	7.60	8.16	66.7	0.15	2.57*
	Rear	20.0 10^{-3}	17.5 4.08	3.78	3.97	66.7	0.15	2.50*

R_0 : Normal operating resistance (Ω)

T_{sc} : Overheat temperature of hot film (c_0)

r_{cs} : Sensitive coefficient of hot film

$$C_s = \frac{R_{100^\circ} - R_0}{100(R_0 - R_{int})}$$

R_{100° : Resistance at 100° c (Ω)

R_0 : Resistance at 0° c (Ω)

R_{int} : Internal resistance of hot film (Ω)

R_{sc} : Functioning resistance, $R_{sc} = (R_{water} - r)(1 + c(T_{sc} - T_{water}))$

where $1 + c(T_{sc} - T_{water}) = \text{overheatratio}$

Table 2: Experimental conditions.

$\mathcal{E}(v)$	$U_{L-P}^{-1/2} \left(\frac{1}{\sqrt{ft} / \text{sec}} \right)$	$(d\mathcal{E}/dU_{L-P})$	$O = B^2 - 4C(\mathcal{E}^2 - A) \sqrt{O}$		$\sqrt{U^{-2}}$ (mv)	$\frac{\sqrt{U^{-2}}}{U_{L-P}}$
101.600	0.5	0.10115	1.9224		1.6	4.60
202.120	0.315	0.03797	1.3865		2.7	7.03
312.365	0.224	0.01712	1.0250		4.5	13.21
402.373	0.220	0.01632	1.0124		4.6	13.63
512.376	0.218	0.01593	0.5151		4.7	13.97
602.443	0.188	0.01009	0.7177		5.9	19.57
702.460	0.180	0.00859	0.4974	0.7053	6.5	22.32
802.473	0.172	0.00713	0.4908	0.7006	6.9	24.52
902.473	0.171	0.00694	0.3365	0.5801	7.0	25.02
1002.480	0.170	0.00675	0.3024	0.5499	7.1	25.76
			0.2726	0.5221		
			0.2680	0.5177		
			0.2563	0.5063		

Table 3

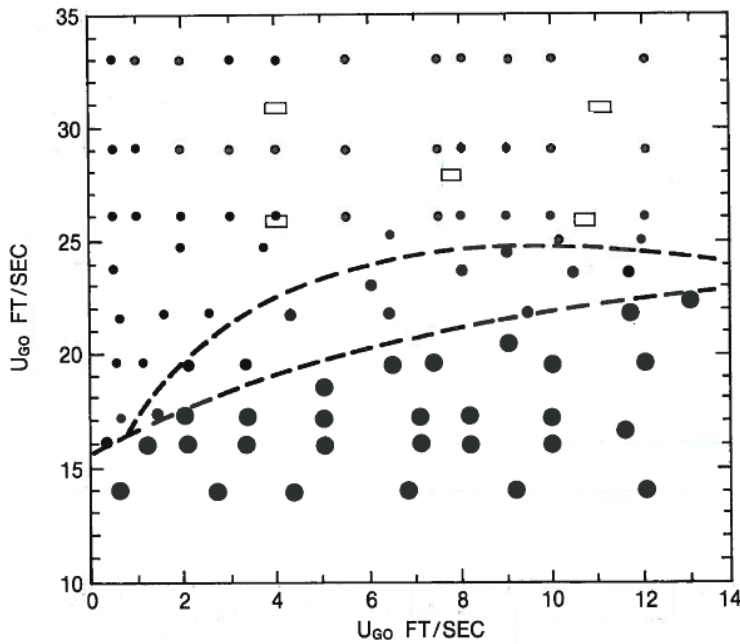


Figure 3 Flow map of horizontal air-water flow.
(8-in. nominal diameter, fully developed flow z/D = 130)

- Slug flow
- Dispersed slug waved flow
- Stratified - dispersed bubbles flow
- Values chosen for experimentation
- Transition zones.

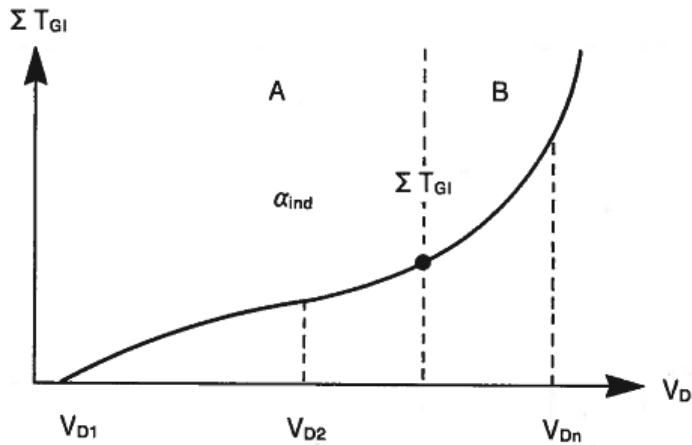


Figure 9. Calibration procedure of hot film for determining void fraction.

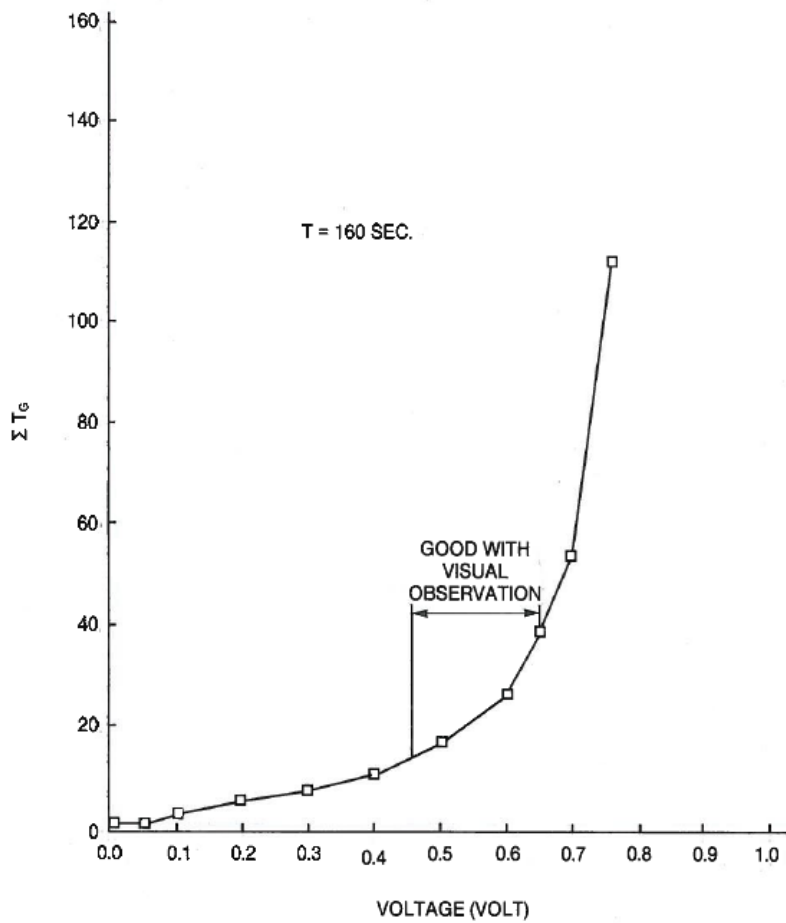


Figure 11: Illustration of void fraction determination with optimum threshold ($z/D=74$, $y/D=0.5$, $X=0.219$, @ 0.610 V DC, void=0.163).

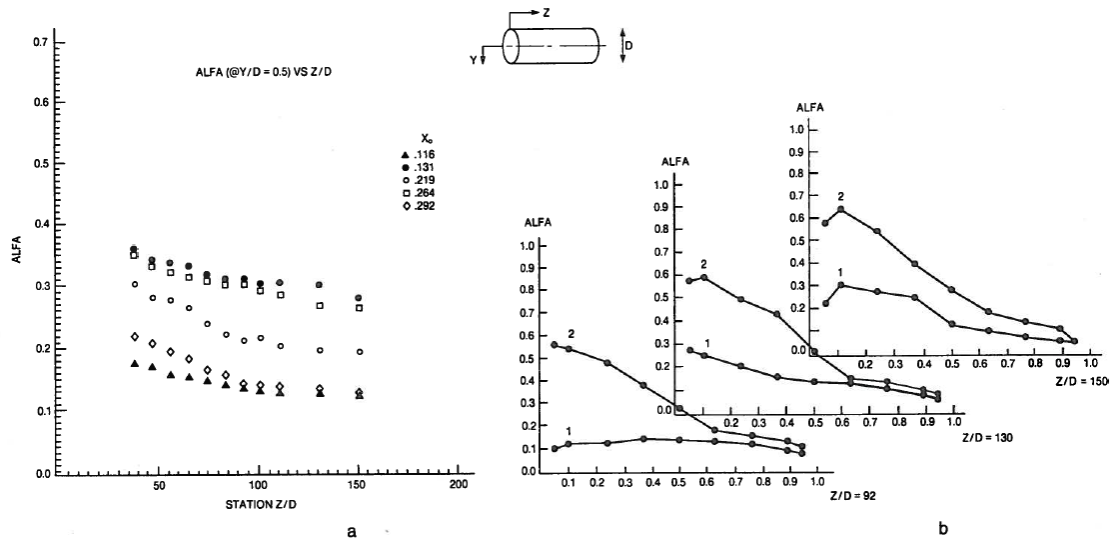


Figure 13: Longitudinal distribution of void fraction for different flow volumetric quality, X_0 :

- a. Void fraction measured at pipe centre line
- b. Void fraction profiles in transversal plane of fully developed flow ($Q_{Lo} = 4373$ USGPM, 1 : $X = 0.116$, 2, $X = 0.264$)

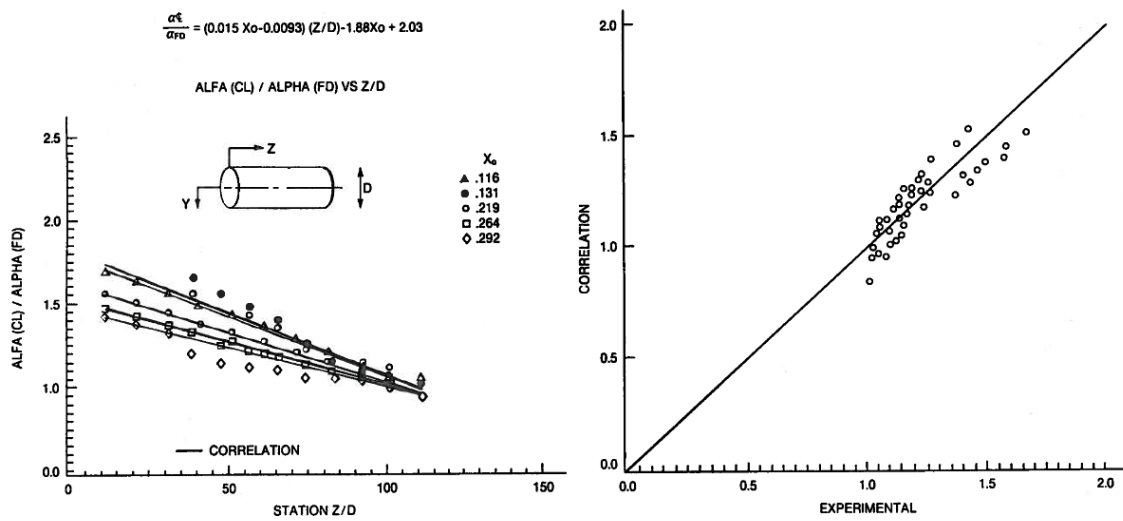


Figure 14: Longitudinal distribution of void centre line / void fully developed flow

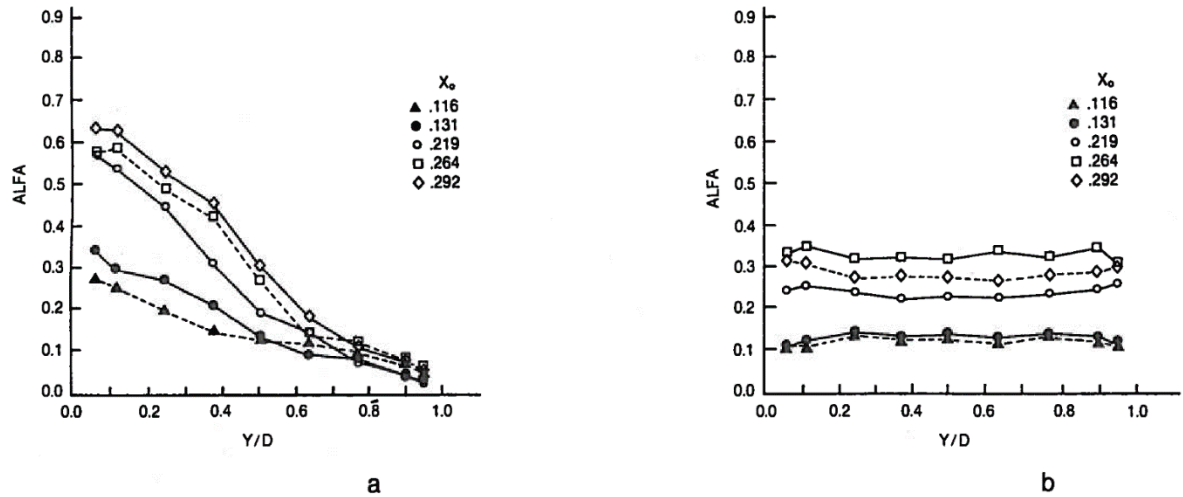


Figure 15: a. Void fraction profiles in transversal plane (see table 1)
b. Void fraction profiles in radial plane (see table 2)

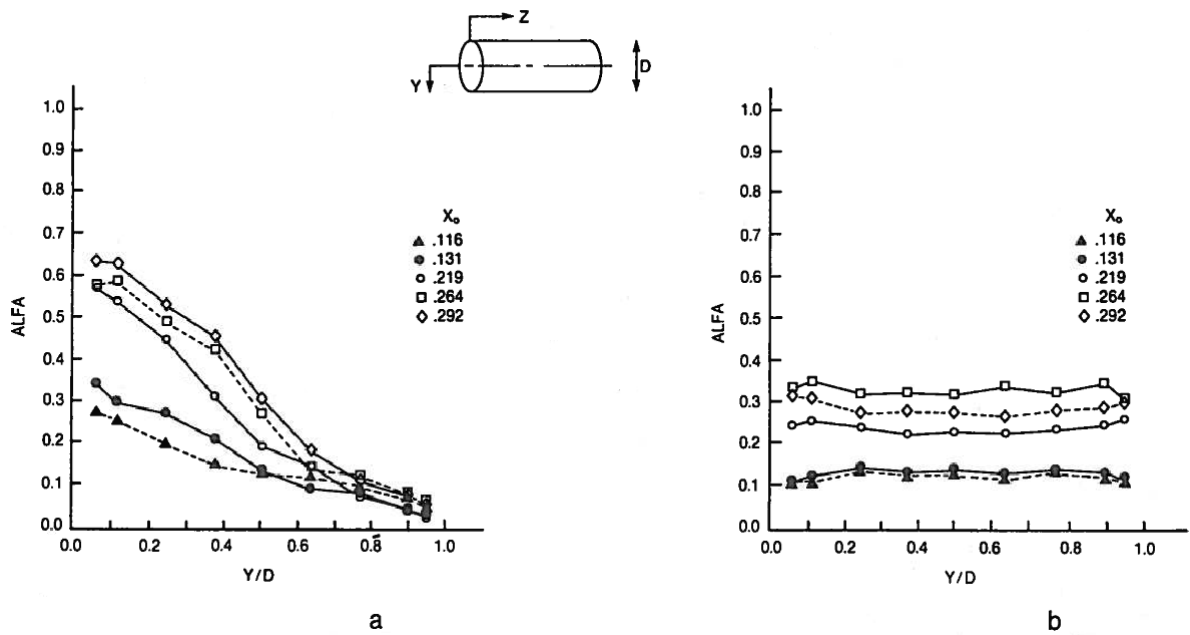


Figure 15: a. Void fraction profiles in transversal plane (see table 1)
b. Void fraction profiles in radial plane (see table 2).

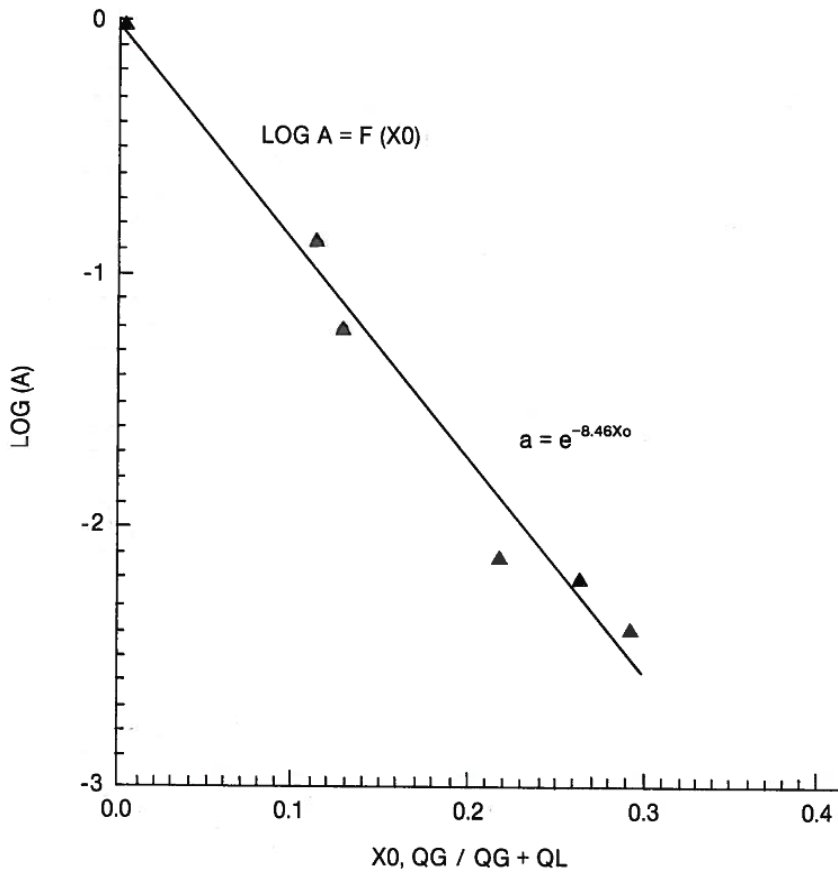


Figure 18: Variation of exponent "a" in power and exponential model of void fraction in terms of flow volumetric quality X_0 .

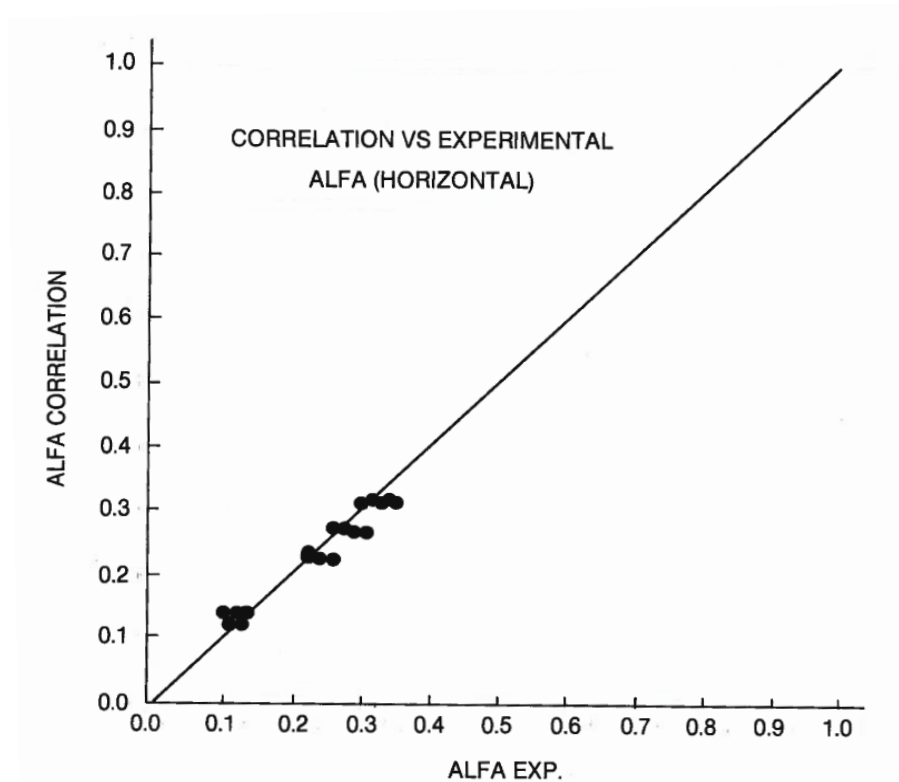


Figure 20: Comparison between experimental results and proposed void correlations in radial plane.